IEEE Photonics Journal
An IEEE Photonics Society Publication

Experimental Demonstration of Superconducting Series Nanowire Photon-Number-Resolving Detector at 660 nm Wavelength

Volume 11, Number 1, February 2019

Ruiying Xu
Xu Tao
Qi Chen
Xiang Li
Guanghao Zhu
Lin Kang
Labao Zhang
Xiaoqing Jia
Xuecou Tu
Qingyuan Zhao
Biaobing Jin
Weiwei Xu
Jian Chen
Peiheng Wu

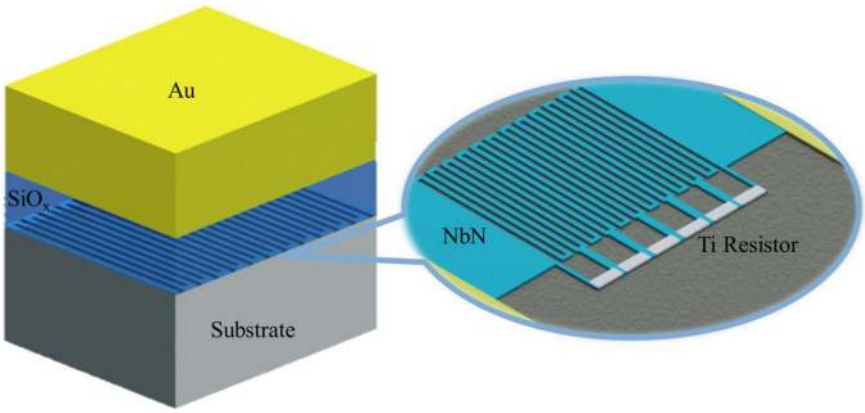

DOI: 10.1109/JPHOT.2019.2894632
1943-0655

IEEE photonics SOCIETY

IEEE

Experimental Demonstration of Superconducting Series Nanowire Photon-Number-Resolving Detector at 660 nm Wavelength

Ruiying Xu, Xu Tao, Qi Chen, Xiang Li, Guanghao Zhu, Lin Kang, Labao Zhang, Xiaoqing Jia, Xuecou Tu, Qingyuan Zhao, Biaobing Jin, Weiwei Xu, Jian Chen, and Peiheng Wu

School of Electronic Science and Engineering, Nanjing University, Nanjing 210093, China

DOI:10.1109/JPHOT.2019.2894632

Manuscript received July 15, 2018; revised December 30, 2018; accepted January 18, 2019. Date of publication January 23, 2019; date of current version February 18, 2019. This work was supported in part by the National Key R&D Program of China under Grant 2017YFA0304002, in part by the National Natural Science Foundation of China under Grant 11227904, Grant 61571105, Grant 61471189, Grant 61571217, Grant 61521001, and Grant 61801206, in part by the National Basic Research Program of China under Grant 2014CB339800, in part by the Fundamental Research Funds for the Central Universities, in part by the Program for Changjiang Scholars and Innovative Research Team in University, and in part by the Jiangsu Key Laboratory of Advanced Techniques for Manipulating Electromagnetic Waves.
Corresponding authors: Guanghao Zhu and Lin Kang (e-mail: ghzhu@nju.edu.cn; kanglin@nju.edu.cn).

Abstract: Photon-number-resolving (PNR) is an important functionality in many applications. The traditional single photon detectors (SNSPDs) operated with the conventional readout scheme does not have the PNR functionality. In this paper, we demonstrate a superconducting photon-number-resolving detector operating at the visible wavelength regime, based on the serial connection of six superconducting nanowires. The results of our 6-element PNR device show clear evidence of *n*-photons differentiation with *n* ranging from 1 to 6. The system detection efficiency reaches 54% with the dark counts rate below 10 Hz at 660 nm. The demonstrated 6-element PNR device does not require a complex readout circuit compared with the SNSPD array device, and is expected to have wider applications in addition to imaging and communication.

Index Terms: Superconducting nanowire detector, photon number resolving, visible wavelength.

1. Introduction

Superconducting nanowire single photon detectors (SNSPDs) [1] have attracted much attention due to their high detection efficiency [2]–[6], low dark counts [7]–[9], and low timing jitter [10], [11]. This makes these detectors promising for free space laser communication [12], quantum key distribution [13], and quantum optics [14].

Photon-number-resolving (PNR) detectors have attracted a large interest in the last decades. Realization of PNR detectors would benefit many applications such as linear-optics quantum computing [15], laser radar [16], [17] and quantum communication [9], [10]. The traditional SNSPDs operated with the conventional readout scheme do not have the PNR functionality [1]. Because the nanowire resistance after single or multiple photon(s) absorption ($\sim 10^3\ \Omega$) is far greater than

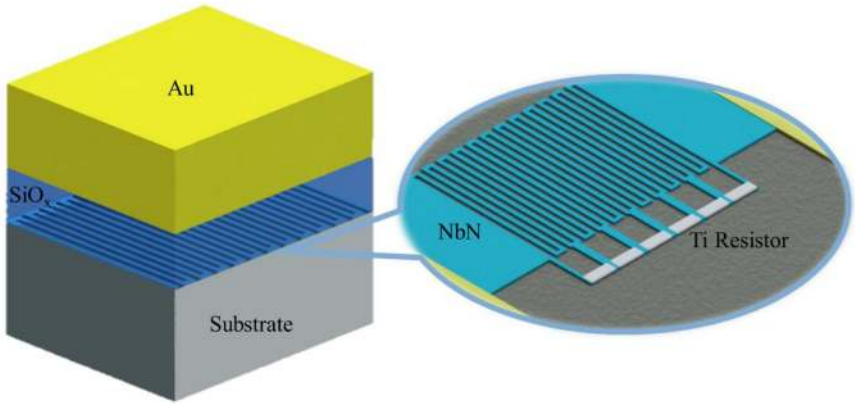

Fig. 1. Schematic diagram of the reported 6-element SND. Inset on the right shows the six nanowire segments in parallel to six Ti resistors.

the load resistance (50 Ω), the whole bias current is diverted into the load resistance. Therefore, the amplitude of the output voltage pulse is not affected by the number of the absorbed photons. A solution was demonstrated by Dauler et al. and Zhao et al. respectively, to the SNSPD array based on spatial multiplexing [18], [19]. However, each pixel requires a separate readout circuit, which increases the complexity of the experiment. Moreover, the extended readout circuits also make the scaling to large photon numbers very difficult. For these reasons, an alternative technique using array of parallel connected superconducting nanowire elements (parallel nanowire photon-number-resolving detector, PND) has been proposed [20]. However, the PND suffers from the current redistribution issue due to its parallel configuration. When one or more photon(s) arrive at a nanowire element, the bias current on the triggered nanowire segment is diverted into the untriggered segments, leading to false counts and limited dynamic ranges.

To overcome the limitation of PND, recently, Jahanmirinejad *et al*. have proposed a device structure called series nanowire detector (SND) [21], [22]. The SND consists of a serial connection of n nanowires, each of which is in parallel to a resistor. Because the nanowire elements are connected in a serial manner, the current redistribution issue of the PND is eliminated. At present, reports on SND are mainly focused on telecommunication wavelength [22]–[25], and reports on the visible wavelength have not been presented. In this article, we demonstrate a photon-number-resolving detector based on SND in visible wavelength. The PNR dynamic range of our SND is six photons. According to measurement results, the amplitude of the output pulse varies linearly with respect to the number of the absorbed photons ($1 \leq n \leq 6$), in good agreement with the numerical simulation. In addition, other basic properties of the device have also been characterized. Our device can achieve 52% system efficiency at 660 nm wavelengths with a dark counts rate at 10 Hz.

2. Device Design and Fabrication

The schematic of the reported device is illustrated in Fig. 1. It consists of a quartz substrate, a silicon oxide layer with NbN nanowires and an Au reflector mirror. Since the operating wavelength is 660 nm, we use quartz as the substrate of which the material absorption is absent. The silicon oxide layer and the gold reflector in the upper layer form an optical cavity, which aims to enhance the absorption efficiency of the NbN nanowires.

We use numerical simulations to determine the optimized parameters for devices designed at 660 nm. The numerical simulation is carried out using FDTD solutions, a software that is available off-the-shelf commercially. The NbN nanowire has a thickness of 7 nm, a width of 80 nm, and a pitch of 240 nm respectively. The thickness of the top Au mirror is 200 nm. The thickness of the upper silicon oxide is optimized by the simulation, so that the maximum absorption efficiency of the

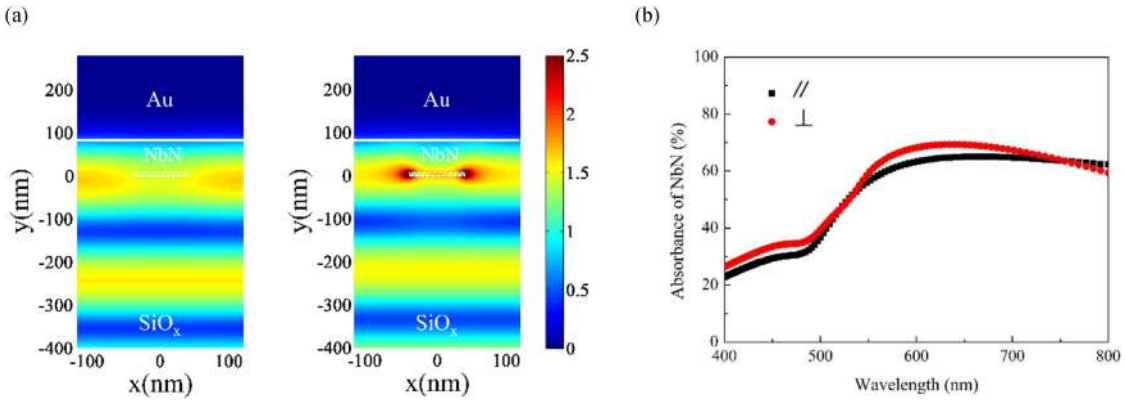

Fig. 2. Numerical simulation results of the device. (a) The spatial distribution of the electric field intensity for case of parallel polarization (left) and perpendicular polarization (right) respectively. (b) The absorption efficiency curve as a function of the wavelength for the designed 660 nm device. Red curve: perpendicular polarization. Black curve: parallel polarization.

device at the target wavelength of 660 nm is reached. The refractive indices of all materials used in the simulation are from FDTD Solutions's material library except NbN, of which the refractive index is a Drude model fitted at room temperature based on ellipsometer measurements [26]. For a quick reference, their refractive indices at 660 nm are $n_{Au} = 0.11 + 3.46i$, $n_{SiOx} = 1.45$ and $n_{NbN} = 2.79 + 3.73i$, respectively. For the simplification of the simulation, we assumed the incident light to illuminate from the quartz substrate, and light reflection from the back side of the quartz substrate is not considered. According to the simulation result, the optimum thickness of the silicon oxide layer is determined to be 80 nm for our targeted 660 nm device. Fig. 2(a) plots the intensity distributions of the electrical fields inside the SNSPD for cases of parallel (left) and perpendicular (right) polarizations respectively, obtained with the excitation wavelength being fixed at 660 nm. The corresponding absorption spectral curves as a function of wavelength for cases of parallel and perpendicular polarizations are plotted in Fig. 2(b). Because the permittivity constant of the NbN at 660 nm (∼20) has a much smaller modulus than that of 1550 nm (∼60), the absorbance curves shows much less sensitivity with respect to the states of the light polarization [30]. Results of the simulation show that, for wavelengths ranging from 560 to 800 nm, the absorption is higher than 58%, and the maximum absorption efficiency of 71% is observed at the wavelength of 660 nm. The moderately high absorption efficiency is due to the fact that the condition of critical coupling is not achieved in the optical cavity sketched in Fig. 1. To increase the absorption efficiency, a partial reflection layer made of high-refractive index material (such as Si) can be added into the quartz substrate. According to our numerical simulation, the absorption efficiency of the device with a carefully tuned partial reflector can reach 94%. Note that in this demonstration, the partial reflector is not adopted for purpose of simplicity.

Besides the optical simulation, the electrical performance of our 6-element SND is also simulated with LTSpice [31]. A schematic diagram of the equivalent circuit for the 6-element SND is shown in Fig. 3(a). Six segments of nanowires are connected in serial, with each nanowire segment being connected in parallel to an on-chip resistor R_p. The superconducting nanowire is electrically modelled as an inductor (L_k) in series to a switched resistor R_n. The working principle of each segment is similar to a standard SNSPD. When no photon arrives, the nanowire stays superconducting and the bias current I_B flows through the nanowire. After a photon is absorbed, the nanowire is switched to the normal state ($\sim 10^3\ \Omega$) and the bias current is diverted into the resistor R_p. The number of the resistor R_p on the pathway of the diverted bias current depends on the nanowire elements that are triggered. In this manner, the amplitude of the output pulse of the SND is proportional to the number of the detection photons, i.e., the functionality of pulse-number-resolving. In the simulation, a constant bias current was carried out for each nanowire segment. The bias current I_B was set

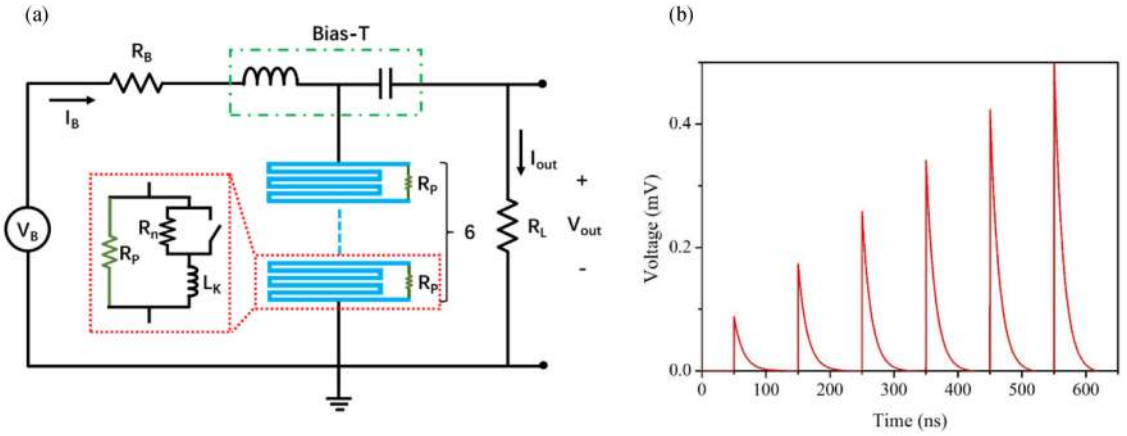

Fig. 3. Simulated electrical performance of the reported device. (a) Equivalent circuit diagram of the 6-element SND. (b) Transient response of the 6-element SND.

at 12.2 μA and the load resistance R_L was 50 Ω. The parallel resistance R_p and the dynamic inductance of the nanowire element L_k were 50 Ω and 100 nH respectively. To emulate multi-photon absorption process, the nanowire segments were triggered at every 100 ns interval and the number of nanowire segments subject to the trigger is increased from 1 to 6. Fig. 3(b) shows the simulated waveform of the output voltage pulse of the 6-element SND, from which it can be seen that when the incident photon number increases, the output pulse amplitude also increases linearly.

Based on the emulation and simulation detailed above, the corresponding 6-element SNDs operating at 660 nm are fabricated. The fabricated devices employ a 500 μm thick quartz as the substrate. A 7 nm thick NbN film is deposited by means of room temperature DC magnetron sputtering. The superconducting transition temperature of the film is 8.1 K. The meander patterns are fabricated by electron beam exposure and reactive ion etching. The NbN nanowires has a width of 80 nm and a pitch of 240 nm respectively, and covers an effective area of 15 μm by 18 μm. After that, six parallel Ti resistors (60 nm thick Ti film) are fabricated by DC magnetron sputtering and lift-off. Upon the completion of the resistors, a layer of amorphous silicon is grown at 50°C with the help of plasma enhanced chemical vapor deposition. The thickness of the SiO_x oxidation layer is controlled by adjusting the pressure of the progress gas and the growth time, and is determined to be 80 nm with the help of a nanoscale optical film thickness measurement system (NanoCalc, Ocean Optics). Finally, the device fabrication is completed by depositing a 200 nm thick Au film with the help of AC magnetron sputtering.

Fig. 4(a) shows the scanning electron image of the 6-element SND. The six nanowire segments are highlighted in colors for clarity. The microscope photo of the six parallel Ti resistors is presented in Fig. 4(b). It can be seen from the SEM diagram that our nanowire is very homogeneous and the width of the NbN nanowire is about 79.6 nm, which is the desired width. Note that in order to eliminate the current crowding effect, the nanowire's nook is optimized and the filling factor is chosen as 33% [28].

3. Experimental Setup and Results

The fabricated device is optically packaged by attaching a fiber at the backside of the quartz substrate. With the help of a focusing lens, the coupling efficiency reaches 90%. The packaged device is mounted on a compact Gifford–McMahon cryocooler and cooled to 2.3 K [29]. Fig. 5(a) shows the schematic diagram of the measurement system. The device was current-biased with a low-noise voltage source through the DC port of a bias-tee. The signals from the device were read-out with a low-noise amplifier connected to the RF port of the bias-tee. The amplified pulses

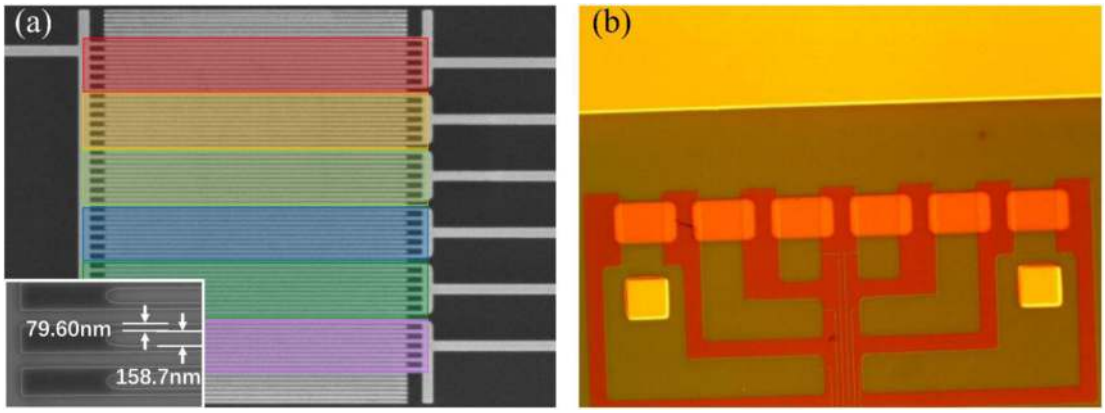

Fig. 4. Scanning electron microscopy image of the 6-element SND. The nanowire width is 79.6 nm with a filling factor of 33%. Each nanowire has been colored for clarity. (b) Optical micrograph of the parallel resistors.

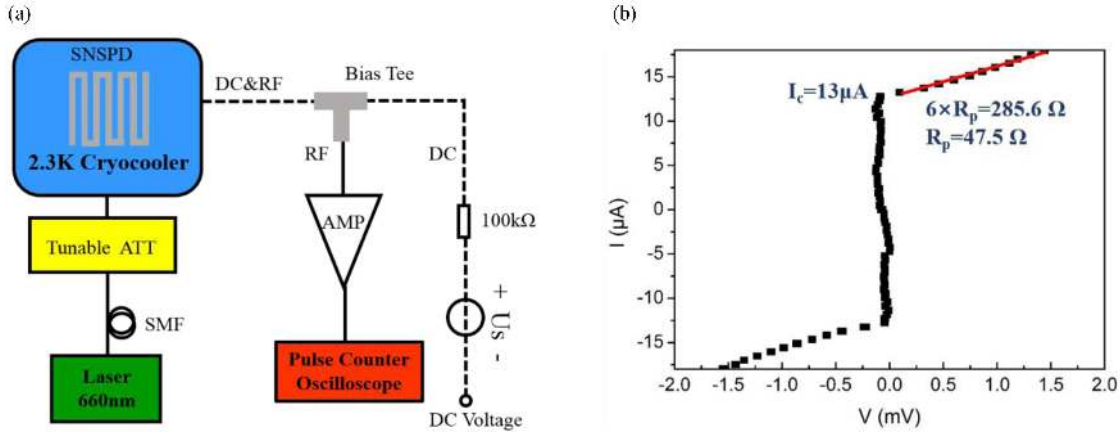

Fig. 5. (a) Schematic diagram of the measurement system. (b) IV characterization of the device. The I_c of the device is 13 μA and the average value of R_p is 47.6 Ω obtained by calculating the reciprocal of the slope.

were counted with a 300-MHz-bandwidth counter. A 33-GHz-bandwidth sampling oscilloscope was used for output pulse waveform characterization. The I-V characteristics are shown in Fig. 5(b). According to the current-voltage (I-V) measurement of the 6-element SND, the critical current I_C of the device is 13 μA and the average value of R_p is 47.6 Ω. For optical characterization, we used a pulsed semiconductor diode laser operating at 660 nm as the photon source. The pulsed laser had a repetition rate of 10 MHz, and the light intensity was adjusted so that each pulse contained only a few photons. We offset the SND device under $I_B = 12.2$ μA. Fig. 6(a) shows the corresponding persistence map measured by the oscilloscope operating in the fluorescent mode. Six pulses with different amplitudes (marked by different colors) can be clearly seen in the figure, showing the PNR functionality. The related histogram is shown in Fig. 6(b). Each peak is fitted with a Gaussian distribution (solid black line), corresponding to the detection of 1 to 6 photons, respectively. The peaks at 28 mV, 59 mV, 90 mV, 122 mV, 149 mV and 177 mV correspond to the amplitude of the output pulse resulted by the detections of 1, 2, 3, 4, 5, and 6 photons respectively.

The PNR functionality of the 6-element SND was further confirmed by measuring the count rate dependence of the input light power. To determine the count rate caused by the event of the detection of $\geq$n photons, the threshold voltage of the counter was chosen as the median value

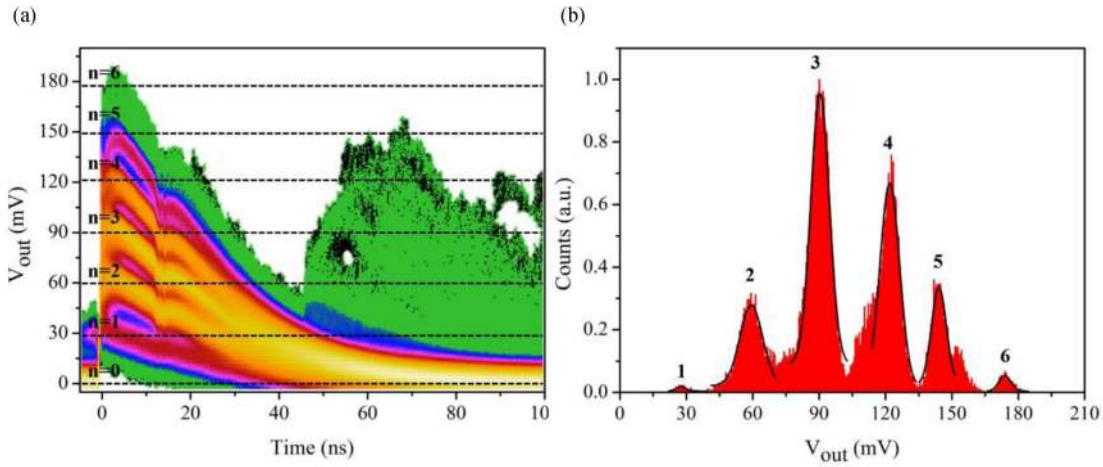

Fig. 6. (a) The oscilloscope persistence map from the sampling oscilloscope (bandwidth: 33 GHz). Different colors representing the number of amplitude pulses that are counted. (b) The corresponding histogram along with the Gaussian fits (black solid line).

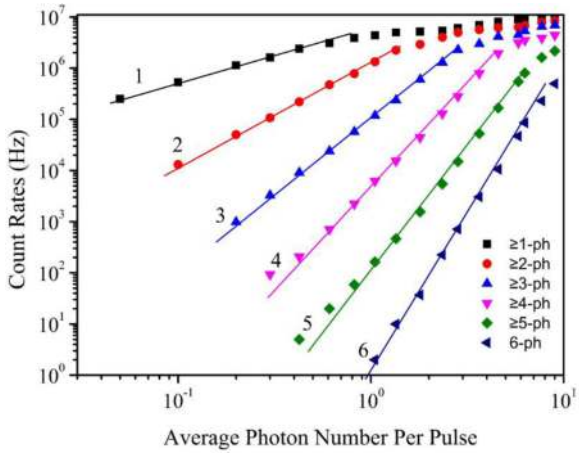

Fig. 7. Count rates of the detection events of at least n photons (n varying from 1 to 6) as a function of the average photon number per pulse. The device was bias at $I_B = 12.2\ \mu$A.

between the (n-1)th and nth peaks shown in Fig. 6(b). Using a set of different threshold voltages described above, the count rates of the detection of $\geq$n photons were measured as a function of the input light power. The results are plotted in Fig. 7, where both the signal counts and the light power are presented in log scales. The solid lines are linear fits to the data with the slopes close to 1, 2, 3, 4, 5 and 6, respectively. Note that when the light power is much below the single photon level, the average photon numbers per pulse μ is far less than 1 [18]. In this small signal region, the count rates of detecting at least n photons should be proportional to μ^n. The results of the fitted slope shown in Fig. 7 agree well with the theoretical analysis, thereby providing a further confirmation of the PNR functionality of our 6-element SND.

The system detection efficiency (SDE) and dark count rates (DCR) were also characterized at a temperature of 2.3 K. When characterizing the efficiency, a low threshold voltage is used for the counter, and the average detected photon number per pulse is adjusted to be $\sim$0.1. Therefore, the SND device essentially operates in the single-photon detection mode and the obtained system efficiency should be close to its real value. Figure 8 shows the SDE and DCR measured as a

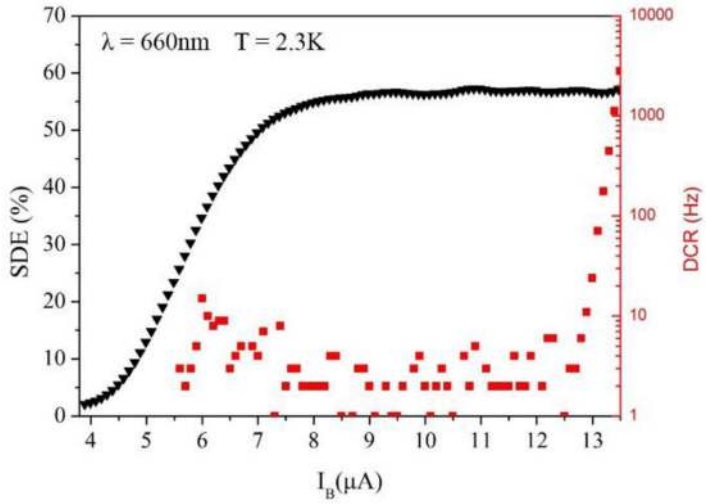

Fig. 8. System detection efficiencies and dark count rates as a function of the bias current at $\lambda = 660$ nm at a temperature of 2.3 K.

function of the bias current. The SDE reaches the maximum value of 54% under a bias current $I_B = 12.5\ \mu$A, with the DCR below 10 Hz at the same time. The SDE curve begins to saturate at $I_B = 8.2\ \mu$A, indicating that the intrinsic efficiency of our device is very close to 100%.

4. Conclusions

In summary, we have demonstrated a photon-number-resolving detector based on SND in the visible wavelength. The results of our 6-element SND show clear evidence of n-photons with n ranging from 1–6. The system detection efficiency reaches 54% with the dark counts rate below 10 Hz at the wavelength of 660 nm. Compared with the SNSPD array device and the PND photon-number resolution device, the SND photon-number resolution device is simple without a complex readout circuit. We believe that this 6-element SND will have wider applications in the future and give impetus to imaging and detection in the visible wavelength. Besides, it will also show extraordinary potential in quantum photonic circuit [32].

References

[1] G. N. Gol'tsman *et al.*, "Picosecond superconducting single-photon optical detector," *Appl. Phys. Lett.*, vol. 79, no. 6, pp. 705–707, 2001.
[2] F. Marsili *et al.*, "Detecting single infrared photons with 93% system efficiency," *Nature Photon.*, vol. 7, no. 3, pp. 210–214, 2013.
[3] W. Zhang *et al.*, "NbN superconducting nanowire single photon detector with efficiency over 90% at 1550 nm wavelength operational at compact cryocooler temperature," *Sci. China Phys. Mech. Astron.*, vol. 60, no. 12, 2017, Art. no. 120314.
[4] D. Rosenberg, A. J. Kerman, R. J. Molnar, and E. A. Dauler, "High-speed and high-efficiency superconducting nanowire single photon detector array," *Opt. Exp.*, vol. 21, no. 2, pp. 1440–1447, 2013.
[5] V. B. Verma *et al.*, "High-efficiency superconducting nanowire single-photon detectors fabricated from MoSi thin-films," *Opt. Exp.*, vol. 23, no. 26, pp. 33792–33801, 2015.
[6] T. Yamashita, S. Miki, H. Terai, and Z. Wang, "Low-filling-factor superconducting single photon detector with high system detection efficiency," *Opt. Exp.*, vol. 21, no. 22, pp. 27177–27184, 2013.
[7] M. K. Akhlaghi, H. Atikian, A. Eftekharian, M. Loncar, and A. H. Majedi, "Reduced dark counts in optimized geometries for superconducting nanowire single photon detectors," *Opt. Exp.*, vol. 20, no. 21, pp. 23610–23616, 2012.
[8] H. Shibata, K. Shimizu, H. Takesue, and Y. Tokura, "Ultimate low system dark-count rate for superconducting nanowire single-photon detector," *Opt. Lett.*, vol. 40, no. 14, pp. 3428–3431, 2015.
[9] C. M. Natarajan, M. G. Tanner, and R. H. Hadfield, "Superconducting nanowire single-photon detectors: Physics and applications," *Supercond. Sci. Technol.*, vol. 25, no. 6, 2012, Art. no. 063001.

[10] E. A. Dauler *et al.*, "Review of superconducting nanowire single-photon detector system design options and demonstrated performance," *Opt. Eng.*, vol. 53, no. 8, 2014, Art. no 081907.
[11] L. You *et al.*, "Jitter analysis of a superconducting nanowire single photon detector," *AIP Adv.*, vol. 3, no. 7, 2013, Art. no. 072135.
[12] D. V. Murphy, J. E. Kansky, M. E. Grein, R. T. Schulein, M. M. Willis, and R. E. Lafon, "LLCD operations using the lunar lasercom ground terminal," *Proc. SPIE*, vol. 8971, 2014, Art. no. 89710V.
[13] H. Takesue *et al.*, "Quantum key distribution over a 40-dB channel loss using superconducting single-photon detectors," *Nature Photon.*, vol. 1, no. 6, pp. 343–348, 2007.
[14] R. H. Hadfield, "Single-photon detectors for optical quantum information applications," *Nature Photon.*, vol. 3, no. 12, pp. 696–705, 2009.
[15] P. Kok, W. J. Munro, K. Nemoto, T. C. Ralph, J. P. Dowling, and G. J. Milburn, "Linear optical quantum computing with photonic qubits," *Rev. Modern Phys.*, vol. 79, no. 1, pp. 135–175, 2007.
[16] W. C. Priedhorsky, R. C. Smith, and C. Ho, "Laser ranging and mapping with a photon-counting detector," *Appl. Opt.* vol. 35, no. 3, pp. 441–452, 1996.
[17] A. M. Wallace, G. S. Buller, and A. C. Walker, "3D imaging and ranging by time-correlated single photon counting," *Comput. Control Eng. J.*, vol. 12, no. 4, pp. 157–168, 2001.
[18] E. A. Dauler *et al.*, "Multi-element superconducting nanowire single-photon detector," *IEEE Trans Appl. Supercond.*, vol. 17, no. 2, pp. 279–284, Jun. 2007.
[19] Q. Zhao *et al.*, "Superconducting-nanowire single-photon-detector linear array," *Appl. Phys. Lett.*, vol. 103, no. 14, 2013, Art. no. 142602.
[20] A. Divochiy *et al.*, "Superconducting nanowire photon-number-resolving detector at telecommunication wavelengths," *Nature Photon.*, vol. 2, no. 5, pp. 302–306, 2008.
[21] S. Jahanmirinejad and A. Fiore, "Proposal for a superconducting photon number resolving detector with large dynamic range," *Opt. Exp.*, vol. 20, no. 5, pp. 5017–5028, 2012.
[22] S. Jahanmirinejad, *et al.*, "Photon-number resolving detector based on a series array of superconducting nanowires," *Appl. Phys. Lett.*, vol. 101, no. 7, 2012, Art. no. 072602.
[23] Z. Zhou *et al.*, "Superconducting series nanowire detector counting up to twelve photons," *Opt. Exp.*, vol. 22, no. 3, pp. 3475–3489, 2014.
[24] F. Mattioli, "Superconducting nanowires connected in series for photon number resolving functionality," *J. Phys., Conf.*, vol. 507, 2014, Art. no. 042024.
[25] F. Mattioli, Z. Zhou, A. Gaggero, R. Gaudio, R. Leoni, and A. Fiore, "Photon-counting and analog operation of a 24-pixel photon number resolving detector based on superconducting nanowires," *Opt. Exp.*, vol. 24, no. 8, pp. 9067–9076, 2016.
[26] X. Hu, "Efficient superconducting-nanowire single-photon detectors and their applications in quantum optics," Ph.D. Dissertation, Massachusetts Inst. Technol., Cambridge, MA, USA, 2011. [Online]. Available: http://18.7.29.232/handle/1721.1/63073
[27] F. Zheng *et al.*, "Design of efficient superconducting nanowire single photon detectors with high polarization sensitivity for polarimetric imaging," *J. Opt. Soc. Amer. B*, vol. 33, no. 11, pp. 2256–2264, 2016.
[28] J. R. Clem and K. K. Berggren, "Geometry-dependent critical currents in superconducting nanocircuits," *Phys. Rev. B*, vol. 84, no. 17, 2011, Art. no. 174510.
[29] R. Xu *et al.*, "Demonstration of polarization-insensitive superconducting nanowire single-photon detector with si compensation layer," *J. Lightw. Technol.*, vol. 35, no. 21, pp. 4707–4713, Nov. 2017.
[30] F. Zheng *et al.*, "Design of a polarization-insensitive superconducting nanowire single photon detector with high detection efficiency," *Sci. Rep.*, vol. 6, 2016, Art. no. 22710.
[31] K. Berggren *et al.*, "A superconducting nanowire can be modeled by using SPICE," *Supercond. Sci. Technol.*, vol. 31, 2018, Art. no. 055010.
[32] E. Schmidt *et al.*, "Photon-number resolving SNSPD for quantum photonic integrated circuits on GaAs at 4.2 K," *arXiv*, vol. 1810, 2018, Art. no. 11256.